Topological magnonic dislocation modes

Carlos Saji [1], Nicolas Vidal-Silva [2], Alvaro S. Nunez [1], and Roberto E. Troncoso [3]
[1]*Departamento de Física, FCFM, Universidad de Chile, Santiago, Chile*
[2]*Departamento de Ciencias Físicas, Universidad de La Frontera, Casilla 54-D, Temuco, Chile*
[3]*Departamento de Física, Facultad de Ciencias, Universidad de Tarapacá, Casilla 7-D, Arica, Chile*

(Received 14 October 2024; revised 29 January 2025; accepted 25 March 2025; published 22 April 2025)

Spin fluctuations in two-dimensional ferromagnets in the presence of crystalline lattice dislocations are investigated. We show the existence of topologically protected nonpropagative modes that localize at dislocations. These in-gap states, termed *magnonic dislocation modes*, are characterized by the Z_2 topological invariant that derives from broken parity symmetry induced by sublattice magnetic anisotropy. We uncover that bulk topology existing in the perfect crystal is robust under the influence of lattice defects, which is monitored by the real-space Bott index. It is also revealed that the topology of magnonic dislocation modes remains unaffected when bulk topology becomes trivial and is remarkably resilient against magnetic disorder. Our findings point to the intriguing relationship between topological lattice defects and the spectrum of topological spin excitations.

DOI: 10.1103/PhysRevB.111.165146

I. INTRODUCTION

Lattice dislocations, structural defects in ordered solids, are irregularities that emerge as abrupt changes in the crystal order. These are characterized by the Burgers vector $\mathbf{B}$ that remains constant over the entire length of the dislocation. Dislocations in solid-state materials have been the ground for a broad range of scopes such as melting [1], elastic response, and thermal conductivity [2]. A renewed interest in dislocations promoted it to a central role in the interplay of real-space topological defects and emergent band topology [3,4]. Concretely, it was shown in topological insulators and superconductors [3,5–17], and mechanical [18–21] and light-based systems [22–25], that a pair of gapless helical modes appear bound to the line defect, which are determined from the index of the dislocation modes [3],

$$\mathrm{N_{dis}} = \frac{1}{2\pi}\mathbf{B}\cdot\mathbf{G}\ (\mathrm{mod}\ 2), \tag{1}$$

where the topology of these modes is protected by the topological $\mathbb{Z}_2$ invariant, $\mathbf{G} = \nu_1\mathbf{b}_1 + \nu_2\mathbf{b}_2$, where ν_i and $\mathbf{b}_i$ are the weak topological index and reciprocal lattice vectors, respectively. Importantly, these states are robust against disorder that preserve the nontrivial bulk topology, following from the bulk-dislocation correspondence [26–28], a remarkable feature that has been experimentally demonstrated in two-dimensional (2D) photonic crystals and metamaterials.

Quantum spin fluctuations of ordered magnets, magnons, inherit fundamental properties from the crystal lattice structure [29,30]. It is encoded in their band spectrum and corresponding interactions with phonons, pointlike defects, and structural disorder. The role of topological lattice defects on the spin-wave fluctuations has been a recurrent issue, particularly on interference and scattering effects [31–34], ferromagnetic resonance (FMR) spectra [35–37], relaxation [38,39] and thermal conductivity [40,41], and recently in helical textures on chiral magnets [42]. Differently, the concept of topology might emerge in the band structure of magnonic states with remarkable signatures such as robust helical edge states and the thermal Hall effect [43,44]. Topological magnons have been strongly scrutinized in a wide variety of spin and lattice systems [43–50], which are characterized by topological invariants that remain unchanged under smooth deformations and set the ground for the bulk-boundary correspondence [51]. The immunity of topological states to disorder, deep rooted to topological matter [52,53], has been tested in collinear magnets [54,55] and glassy skyrmions [56]. However, the influence of crystal lattice defects, such as dislocations, on the band topology is an unexplored arena in magnetic systems with intriguing effects regarding the stability and localization of topological magnon states.

In this paper, we show the existence of topological magnon states bound to the dislocations (see Fig. 1) within the crystal structure of magnetic insulators. Remarkably, it is shown that magnonic dislocation modes are stabilized when parity symmetry is broken and persists while the topological bulk gap is closed. The existing bulk topology is diagnosed by the evaluation of a real-space topological index, the bosonic Bott index, which turns out to be stable in the presence of dislocations. It is shown that dislocation modes and edge modes have different degrees of robustness against disorder. The stability of these states is demonstrated for a model that supports a collinear ferromagnetic phase.

II. SPIN AND LATTICE MODEL

We consider a magnetic system with spins localized on a two-dimensional honeycomb lattice described by the spin Hamiltonian,

$$\mathcal{H}_S = -\sum_{\langle rr'\rangle}\Big\{J\boldsymbol{S}_r\cdot\boldsymbol{S}_{r'} + F(\boldsymbol{S}_r\cdot\mathbf{e}_{rr'})(\boldsymbol{S}_{r'}\cdot\mathbf{e}_{rr'}) + \big[K_r\big(S_r^z\big)^2 - BS_r^z\big]\delta_{rr'}\Big\}, \tag{2}$$

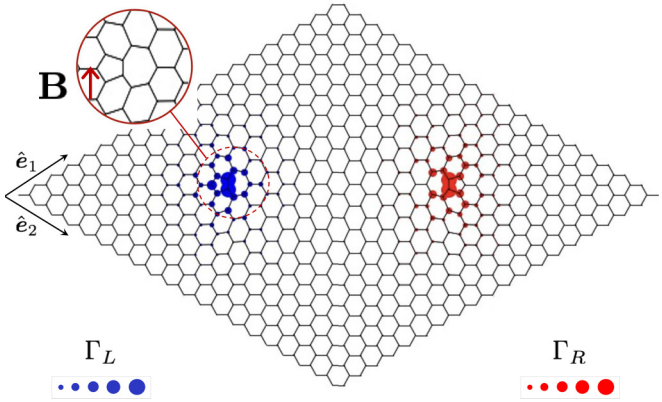

FIG. 1. Schematic representation of a pair of dislocations in the hexagonal lattice with the in-plane Burgers vector $\mathbf{B} = \pm\sqrt{3}\hat{\mathbf{y}}$, at the left and right sides of the dislocations, respectively. The topological magnonic dislocation modes, Γ_L (left) and Γ_R (right) states, are shown localized at the ends of the dislocation. These modes are gapped due to parity symmetry breaking, and their wave-function amplitudes are, accordingly, colored differently.

with the nearest-neighbor exchange coupling J and pseudodipolar interaction with strength F. The last coupling results from the spin-orbit interaction [57,58], where $\mathbf{e}_{\boldsymbol{rr'}}$ is the unit vector that connects the $\boldsymbol{r}$ and $\boldsymbol{r'}$ lattice sites. The easy-axis anisotropy $K_{\boldsymbol{r}}$ at the $\mathcal{A}(\mathcal{B})$ sublattice is parametrized as $K_{\mathcal{A}(\mathcal{B})} = K \pm \Delta_K$, and B is the applied magnetic field along the z direction. The dislocation is introduced following the Volterra process [59]. A set of atoms is removed, resulting in a pentagon-heptagon structure, and thus moving an equal number of steps around the dislocation sets a nonclosed loop defining the Burgers vector (see Fig. 1). It is worth stressing that, although linear dislocations might be more complicated, e.g., curvilinear or multiples, we choose the displayed linear straight dislocation for simplicity. For numerical convenience, we consider a couple of defects that create a pair of dislocations in the bulk of the system. The local lattice deformation produces a distortion of the spin Hamiltonian, $\mathcal{H}_T = \mathcal{H}_S + \mathcal{H}_{\rm dis}$, that gives rise to a magnetoelastic interaction $\mathcal{H}_{\rm dis}$ relating the spin and lattice degrees of freedom. Hereafter, in our numerical calculations, we consider the relevant magnetic parameters with a similar order of magnitude, i.e., $J \sim K \sim \Delta_K$, as typically occurs in van der Waals magnets [60,61].

Quantum spin fluctuations around the ordered ground state are determined by the Hamiltonian of noninteracting magnons using Holstein-Primakoff (HP) bosons [62]. Around the classical magnetic state, z-axis oriented, the HP mapping of spin operators reads $S^+_{\boldsymbol{r}} = (2S - a^\dagger_{\boldsymbol{r}} a_{\boldsymbol{r}})^{1/2} a_{\boldsymbol{r}}$, $S^-_{\boldsymbol{r}} = (2S - a^\dagger_{\boldsymbol{r}} a_{\boldsymbol{r}})^{1/2} a^\dagger_{\boldsymbol{r}}$, and $S^z_{\boldsymbol{r}} = S - a^\dagger_{\boldsymbol{r}} a_{\boldsymbol{r}}$. Thus, expanding the spin operators as a series in $1/S$, the spin Hamiltonian reduces to $\mathcal{H}_T \approx \mathcal{H}_0 + \mathcal{H}_m$, where $\mathcal{H}_0$ is the classical and zero-point energy. In real space the magnon Hamiltonian reads $\mathcal{H}_m = \Psi^\dagger \mathrm{H} \Psi$, where the $2N$-component operator field $\Psi = (a_{\boldsymbol{r}_1} \ldots, a_{\boldsymbol{r}_N}, a^\dagger_{\boldsymbol{r}_1} \ldots a^\dagger_{\boldsymbol{r}_N})^T$, with $\boldsymbol{r}_i$ the lattice position and H the $2N \times 2N$ matrix Hamiltonian, with N the number of lattice sites and tight-binding matrix elements given by

$$\mathrm{H}_{\boldsymbol{rr'}} = \begin{pmatrix} \Omega_{\boldsymbol{rr'}} & \Delta_{\boldsymbol{rr'}} \\ \Delta^*_{\boldsymbol{rr'}} & \Omega^*_{\boldsymbol{rr'}} \end{pmatrix},$$

where $\Delta_{\boldsymbol{rr'}} = -SF(\boldsymbol{e}^- \cdot \mathbf{e}_{\boldsymbol{rr'}})(\mathbf{e}_{\boldsymbol{rr'}} \cdot \boldsymbol{e}^-)\delta_{\langle \boldsymbol{rr'}\rangle}/2$, $\Omega_{\boldsymbol{rr'}} = -S[J + F(\boldsymbol{e}^+ \cdot \mathbf{e}_{\boldsymbol{rr'}})(\mathbf{e}_{\boldsymbol{rr'}} \cdot \boldsymbol{e}^-)]\delta_{\langle \boldsymbol{rr'}\rangle}/2 + S\Lambda_{\boldsymbol{r}}\delta_{\boldsymbol{rr'}}$, $\Lambda_{\boldsymbol{r}} = \sum_{\langle \boldsymbol{rr'}\rangle}\{J\boldsymbol{S}_{\boldsymbol{r}} \cdot \boldsymbol{S}_{\boldsymbol{r'}} + [K_{\boldsymbol{r}}(S^z_{\boldsymbol{r}})^2 - BS^z_{\boldsymbol{r}}]\delta_{\boldsymbol{rr'}}\}$, and $\boldsymbol{e}^\pm = \hat{\boldsymbol{x}} \pm i\hat{\boldsymbol{y}}$. The bosonic Hamiltonian is paradiagonalized by the Bogoliubov transformation $(a_{\boldsymbol{r}}, \ldots, a^\dagger_{\boldsymbol{r}})^T = \mathrm{T}_{\boldsymbol{rr'}}(\alpha_{\boldsymbol{r'}}, \ldots, \alpha^\dagger_{\boldsymbol{r'}})^T$, with T the paraunitary transformation that satisfies $\mathrm{T}^\dagger \zeta \mathrm{T} = \zeta$ to guarantee the commutation relation $[\boldsymbol{\alpha}, \boldsymbol{\alpha}^\dagger] = \mathbb{I} \otimes \sigma_z = \zeta$ for bosonic operators [63] (with σ_z the Pauli matrix). Therefore, the diagonalized magnon Hamiltonian is written as $\mathcal{H}_m = \sum_n \mathcal{E}_n \alpha^\dagger_n \alpha_n$, with $\mathcal{E}_n$ the energy for the nth band.

III. BULK TOPOLOGY

Ferromagnetic honeycomb defect-free lattices, described by the spin Hamiltonian in Eq. (2), exhibit topological magnonic phases featured by the Chern number [50,54,58]. The topological gap Δ_b is induced by the pseudodipolar interaction F and controlled by the sublattice easy-axis anisotropy Δ_K. We now determine the bulk topology when dislocations are present. Since crystalline symmetry is locally broken, we evaluate the topology of magnonic bands through the bosonic Bott index [54]. It is a real-space topological invariant that is equivalent to the Chern number in the thermodynamic limit and when translational invariance is restored [64–66]. For the set of eigenstates $\{\mathcal{E}_n\}$, it is defined as $\mathcal{B}(\mathcal{E}_n) = \mathrm{Im}\{\mathrm{Tr}[\log(V_Y V_X V_Y^\dagger V_X^\dagger)]\}/2\pi$, where V_X and V_Y are unitary matrices defined by

$$Pe^{i\pi\Theta}P = \mathrm{T}\zeta \begin{pmatrix} 0 & 0 \\ 0 & V_\Theta \end{pmatrix} \mathrm{T}^\dagger \zeta, \tag{3}$$

with $\Theta = X, Y$ the position operators, represented by matrices where the elements are in a normalized lattice position. The projector $P = \mathrm{T}\zeta\Gamma_{\mathcal{N}}\mathrm{T}^\dagger\zeta$ on states $\{\mathcal{E}_n\}$ and the diagonal matrix $[\Gamma_{\mathcal{N}}]_{nn'} = \gamma\delta_{nn'}$, with $\gamma = 0$ for $\mathcal{N} < n$, and $\gamma = 1$ when $1 \leqslant n \leqslant \mathcal{N}$ [67]. For clean systems, the Bott index of each band is well defined and is an integer as long as $V_Y V_X V_Y^\dagger V_X^\dagger$ is nonsingular. In particular, $\mathcal{B} = 0$ when V_X and V_Y commute and the corresponding band is topologically trivial.

We now consider the effects of dislocations on the band structure and topology of magnonic states. First, in the perfect hexagonal crystal, the two-band spectrum of topologically trivial and nontrivial magnon excitations are displayed at Figs. 2(a) and 2(e), respectively. Note that the trivial gap, induced at the Dirac point, is the result of breaking the parity symmetry by the sublattice anisotropy difference Δ_K. In the presence of dislocations, two interesting effects are highlighted from the magnonic spectrum displayed in Figs. 2(b) and 2(f). First, the bulk topology prevails since a nonzero Bott index is found for the top ($\mathcal{B}_u = -1$) and bottom ($\mathcal{B}_l = +1$) bands, for $F > 0$ and different dislocation lengths [see Fig. 2(f)]. In particular, the Bott index vanishes when $F = 0$ and the bulk topology becomes trivial as expected [see Fig. 2(b)]. Second, a pair of gapped *magnonic dislocation modes* appear inside the gap, Δ_b, and are bound to the ends of the dislocation, indicated by the black dots in the inset of Fig. 2(b). The gap between these states, $\Delta_{\rm dm}$, is induced by nonzero values of Δ_K, which is independent of the pseudodipolar coupling, and therefore becomes gapless once the parity symmetry is restored [see the inset of Fig. 2(f)]. It is

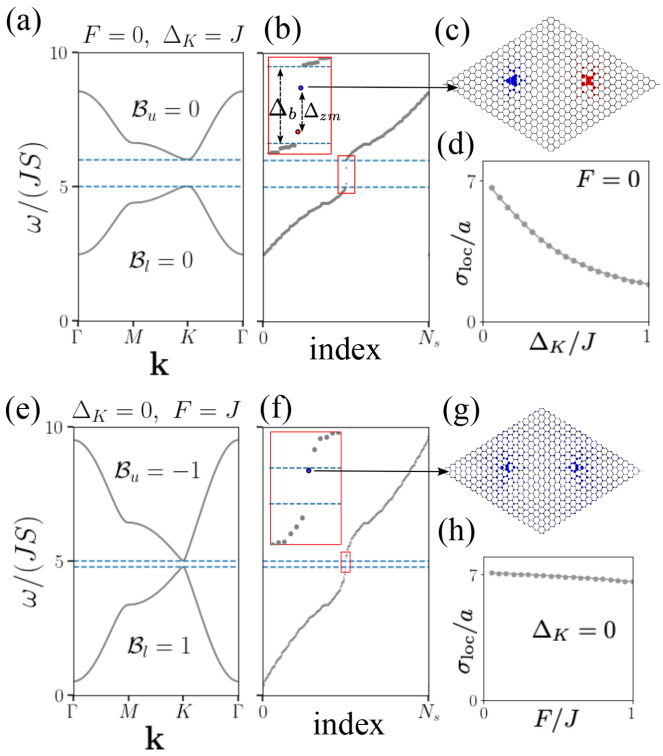

FIG. 2. Top panel: Magnon spectrum for $S = 1$, $K = 2J$, $F = 0$, $\Delta_K = J$, and $B = 0$. Bottom panel: Magnon spectrum for $S = 1$, $K = 2J$, $F = J$, $\Delta_K = 0$, and $B = 0$. (a) and (e) Bulk energy spectrum without dislocation along high-symmetry points in the Brillouin zone. The Bott index for the lower and upper bulk bands satisfies $\mathcal{B}_u = -\mathcal{B}_l = 0$ and $\mathcal{B}_u = -\mathcal{B}_l = -1$ in (a) and (e), respectively. (b) and (f) Magnonic energy spectrum with periodic boundary conditions (PBCs) in the presence of a dislocation pair. The energies of the dislocation modes are within the band gap. (c) and (g) Real spatial amplitude of the dislocation mode wave function $\Gamma_{L,R}(\boldsymbol{r})$. (d) and (h) Real-space localization $\sigma_{\rm loc}$ of $\Gamma_L(\boldsymbol{r})$ as a function of Δ_K/J and F/J, respectively.

worth noting that for a strip geometry, we find that the energy of dislocation modes coexists with those of topological edge states in the presence of pseudodipolar energy, where open boundary conditions (OBCs) along the $\hat{e}_1$ axis are assumed, as is shown in Fig. 2(b).

Magnonic dislocation modes are localized at the ends of the dislocation. Their spatial localization, displayed in Fig. 2, is determined from the overlap, $\Gamma_n(\boldsymbol{r}) = |\langle \mathrm{GS}|a_{\boldsymbol{r}}\alpha_n^\dagger|\mathrm{GS}\rangle|^2$, between the local excitation and the eigenstates, with $|\mathrm{GS}\rangle$ the ground state of the magnon Hamiltonian. We denote $\Gamma_{L,R}(\boldsymbol{r})$ as the magnonic contribution of the left- and right dislocation mode wave functions, displayed in Figs. 1 and 2. The magnonic dislocation modes are nonpropagating states, strongly bound to the lattice dislocation with localization length $\sigma_{\rm loc}$. For a strip geometry, assuming finite size along the $\hat{\boldsymbol{e}}_1$ direction, the corresponding eigenstates for the dislocation modes are displayed in Figs. 2(c) and 2(g). In Fig. 2(d), we plot the characteristic localization length of the wave function around the dislocation as a function of Δ_K. It is defined $\sigma_{\rm loc} = \int |\boldsymbol{r} - \boldsymbol{r}_{\rm dis}||\psi(\boldsymbol{r})|^2\, d^2r$, where we choose $\psi(\boldsymbol{r}) = \Gamma_{L,R}(\boldsymbol{r})$ for the magnonic wave function and $\boldsymbol{r}_{\rm dis}$ the position of the dislocation. Interestingly, the magnonic zero-mode wave function tends to delocalize as Δ_K becomes null, corresponding to the magnonic dislocation modes becoming gapless [see Figs. 2(d) and 2(h)]. Importantly, we remark that while the pseudodipolar interactions play a critical role in stabilizing the bulk topological modes, it is not necessary in a minimal model to give rise to topological dislocation magnon modes as long as the sublattice-breaking anisotropy is present [see Fig. 2(c)]. The pseudodipolar interaction introduces additional symmetry-breaking terms that strengthen the stability of the dislocation modes.

IV. WEAK TOPOLOGY AND $\mathbb{Z}_2$ INVARIANT

We now establish the topological properties of magnon modes bound to the lattice dislocations. The topology of the magnonic dislocation modes is determined by the $\mathbb{Z}_2$ topological index $\mathbf{G}$ which, through Eq. (1), determines the number of modes appearing at the dislocation. The $\mathbb{Z}_2$-invariant and weak topological indices, ν_1 and ν_2, are found through the bulk polarizations, defined as the sum of the Wannier centers,

$$p_x(k_y) = \sum_j \nu_x^j(k_y) \pmod 1, \tag{4}$$

$$p_y(k_x) = \sum_j \nu_y^j(k_x) \pmod 1, \tag{5}$$

which are determined by diagonalizing the Wilson loop matrix, $W_{\boldsymbol{k}}|\nu_{\boldsymbol{k}}^j\rangle = e^{2\pi i \nu_x^j(k_y)}|\nu_{\boldsymbol{k}}^j\rangle$, defined by the product

$$\mathcal{W}_{k_x} = F_{k_x+(N_x-1)\Delta k_x,k_y} \cdots F_{k_x+\Delta k_x,k_y} F_{k_x,k_y}, \tag{6}$$

where $[F_k]^{mn} = \langle u^m_{k_x+\Delta k_x,k_y} \mid u^n_{k_x,k_y}\rangle_{\rm para}$ are the overlaps through the discrete path $k_j = k_x + j\Delta k_x$. The weak topological nature of the system is determined by the winding of the Wilson loops along certain reciprocal lattice directions. The Wilson loop, calculated as the phase evolution of eigenstates over a closed trajectory in momentum space, provides a measure of the actual topological invariant. For dislocation-bound modes, the weak topological invariant, derived from the Wilson loop, ensures the existence of states localized at the dislocation. These states arise because the dislocation *cuts through* the crystal, exposing a one-dimensional topological invariant encoded in the bulk. This mechanism is distinct from strong topology, which relies on the presence of robust edge states in 2D systems. Here, we employ this formulation to compute numerically the Wannier centers $\nu_{x,y}^j$ and therefore the polarizations $p_x(k_y)$ and $p_y(k_x)$. In Fig. 3, we show the polarizations $p_{x,y}$ evaluated for two scenarios, $K = 2J$, $\Delta_K = 0$, $F = 1$, $B = 0$, where bulk topology is nontrivial ($F > 0$) and parity symmetry is preserved ($\Delta_K = 0$), and $K = 2J$, $\Delta_K = J$, $F = 0$, $B = 0$, where bulk topology is trivial ($F = 0$) and parity symmetry is broken ($\Delta_K > 0$). In all plots we assumed $J = 1$.

On the other hand, the polarization is related to the Zak phase as follows. Here, $p_\mu(k_{x,y}) = \frac{i}{2\pi}\int \sum_n \mathcal{A}_{n,\mu}(\boldsymbol{k}) dk_{y,x}$, where $\mathcal{A}_{n,\mu}(\boldsymbol{k}) = \mathrm{Tr}[\Gamma_n \Sigma_z T_{\boldsymbol{k}}^\dagger \Sigma_z \partial_{k_\mu} T_{\boldsymbol{k}}]$ is the Berry connection, with $\Sigma_z = \sigma_0 \otimes \sigma_z$, and the summation runs over the lower bands (below the gap). A quantized polarization indicates that the system lies in a topological phase and provides

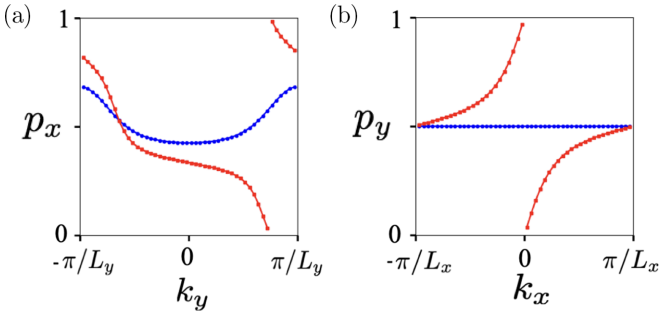

FIG. 3. (a) Polarization $p_x(k_y)$ and (b) polarization $p_y(k_x)$, for the cases with trivial bulk topology $K = 2J$, $\Delta_K = J$, $F = 0$, $B = 0$ (blue line), and the bulk topology is nontrivial trivial $K = 2J$, $\Delta_K = 0$, $F = J$, $B = 0$ (red line). In all plots we assumed $J = 1$.

information about high-order topological magnonic states [68]. Moreover, the weak $\mathbb{Z}_2$ invariants in Eq. (1) can also be computed through the Zak phase [9],

$$\nu_\mu = \frac{i}{\pi}\int_{\mathcal{C}_\mu}\sum_n \mathcal{A}_n(\boldsymbol{k})\cdot d\boldsymbol{k}, \tag{7}$$

where the 1-cycles $\mathcal{C}_x = \mathrm{BZ}|_{k_x=\pi/L_x}$ and $\mathcal{C}_y = \mathrm{BZ}|_{k_y=\pi/L_y}$ run along the k_x and k_y directions in the Brillouin zone, respectively. In particular, we have that $\nu_{x,y} = 2p_{x,y}$ ($k_{y,x} = \pi/L_{y,x}$), and according to the previous numerical calculations (see Fig. 3), we deduce that $(\nu_x, \nu_y) = (0, 1)$, and hence the $\mathbb{Z}_2$-weak invariant is $\mathbf{G} = \boldsymbol{b}_y = \frac{2\pi}{\sqrt{3}}\hat{\mathbf{y}}$. On the other hand, the Burgers vector is given by $\mathbf{B} = q(\boldsymbol{a}_2 - \boldsymbol{a}_1) = q\sqrt{3}\hat{\mathbf{y}}$, where $q = \pm 1$ is the charge of the dislocation (see Fig. 1). Finally, we arrive at $\mathrm{N}_{\mathrm{dis}} = \pm 1$, which is nontrivial. Therefore, there must be a topologically protected dislocation mode, as we claimed.

V. ROBUSTNESS AGAINST DISORDER

Thermal fluctuations, noise, and disorder are ubiquitous and might cause negative effects on the robustness of topological properties. We now discuss the stability of existing topologically protected magnon modes at the dislocation against magnetic disorder. The disorder is modeled by a random out-of-plane magnetic field across the sample, $\mathcal{H}_{\mathrm{random}} = \sum_i \chi S_i^z$, where $\chi \in [-\eta, \eta]$ is a random number and η is the disorder strength. Although general models for disorder would provide a more realistic representation of imperfections, the choice of $\mathcal{H}_{\mathrm{random}}$ is made for its simplicity and to capture the robustness effects of topological modes. A systematic analysis of disorder is left for future studies. A disorder-averaged magnon spectrum as a function of disorder strength η is depicted in Fig. 4. The results are averaged over $n = 20$ realizations of disorder in the spin lattice, where we set the anisotropy and the sublattice anisotropy difference at $K = 2J$ and $\Delta_K = J$, respectively. Magnonic dislocation modes are remarkably robust against the effect of disordered magnetic impurities with considerable strength, resulting from topological protection. The energy of these states remains isolated within the magnon gap Δ_b, avoiding hybridization with bulk states. Although translational symmetry is broken by the presence of disorder, the localization of magnon modes

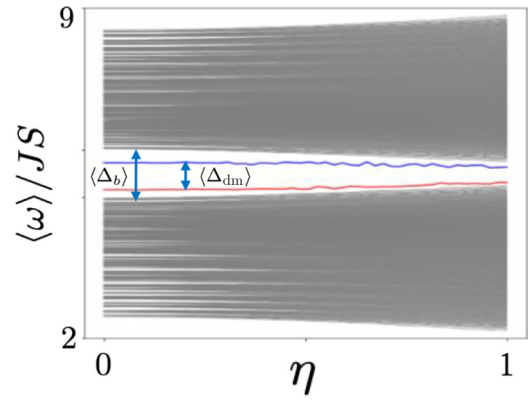

FIG. 4. The energy spectrum of magnons as a function of disorder strength η averaged over 20 realizations with parameters $S = 1$, $K = 2J$, $F = 0$, $\Delta_K = J$. Energy gaps associated with both bulk and magnonic dislocation modes are depicted in blue and red lines.

at the dislocation is not disrupted and their spatial distribution prevail.

VI. DISCUSSION AND CONCLUSIONS

The experimental realization of topological magnonic dislocation modes might settle in two stages: first, the control of the geometrical properties of dislocations, and second, on the actual excitation and local detection of different magnonic states. Advances in manufacturing and imaging techniques allow for a feasible control of dislocation densities [69,70] on the lattice, where various techniques such as X-ray Tomographic Microscopy, scanning tunneling microscopy (STM), and antiferromagnetism (AFM) would enable the real-time observation of dislocations [69–73]. For instance, dislocations in van der Waals magnets (e.g., CrI_3 or Fe_3GeTe_2) could be engineered through techniques such as focused ion beam milling [74] or controlled crystal growth that introduces and controls topological lattice defects [75,76]. In addition, the control of dislocation densities over such materials can be engineered by external strains [77,78]. Magnonic dislocation modes, as well as other states, can be excited by time-dependent (rf) magnetic fields, where their detection could be achieved by quantum metrology techniques [79,80], such as nitrogen-vacancy (NV) centers, which are spin sensors that provide local monitoring of the spatial localization of the wave function near the dislocations. Matching with the frequency of other magnonic states would allow to detect their coexistence with topological edge states.

Although some features of the dislocation mode, such as its localized nature and topological protection, are reminiscent of phenomena in electronic systems, the magnonic system exhibits distinct physics due to their bosonic nature. Magnons are nonconserved quasiparticles whose lifetime and thermal population depend on external driving and dissipation mechanisms, leading to nonequilibrium dynamics of the topological modes that are fundamentally different from their electronic counterparts. Also, the localized nature of the topological dislocation modes could facilitate potential advantages in spintronics, as a magnonic emitter where the mode serves as a controllable source of spin waves. Moreover, the topological

protection of the mode may allow for robust, low-dissipation energy transport, which is particularly desirable for magnon-based devices. Lastly, the magnon spectrum is highly tunable via external magnetic fields, mechanical strains, and temperature, enabling versatile control of the topological properties.

In summary, we have shown that bulk topology prevails in the presence of linear topological defects and dislocations in 2D hexagonal lattices. In addition, such defects induce magnonic states bound at the ends of dislocations. These states are topologically protected and classified by the $\mathbb{Z}_2$ invariant, stabilized by the breaking of parity symmetry and existing even for trivial bulk topology. At the dislocation, the pair of gapped localized topological modes is determined by the relation between the Burgers vector and the topological $\mathbb{Z}_2$ invariant. The presented model is general and might be employed to other forms of magnetic order.

ACKNOWLEDGMENTS

C.S. thanks the financial support provided by ANID National Doctoral Scholarship No. 21210450. R.E.T. thanks funding from Fondecyt Regular 1230747. A.S.N. acknowledges funding from Fondecyt Regular 1230515. N.V.-S. thanks funding from Fondecyt Iniciacion 11220046 and regular 1250364.

[1] D. R. Nelson and B. I. Halperin, Dislocation-mediated melting in two dimensions, Phys. Rev. B **19**, 2457 (1979).
[2] J. Friedel, *Dislocations*, Addison-Wesley Series in Metallurgy and Materials (Pergamon Press, New York, 1964).
[3] Y. Ran, Y. Zhang, and A. Vishwanath, One-dimensional topologically protected modes in topological insulators with lattice dislocations, Nat. Phys. **5**, 298 (2009).
[4] Z.-K. Lin, Q. Wang, Y. Liu, H. Xue, B. Zhang, Y. Chong, and J.-H. Jiang, Topological phenomena at defects in acoustic, photonic and solid-state lattices, Nat. Rev. Phys. **5**, 483 (2023).
[5] J. C. Y. Teo and C. L. Kane, Topological defects and gapless modes in insulators and superconductors, Phys. Rev. B **82**, 115120 (2010).
[6] K.-I. Imura, Y. Takane, and A. Tanaka, Weak topological insulator with protected gapless helical states, Phys. Rev. B **84**, 035443 (2011).
[7] D. Asahi and N. Nagaosa, Topological indices, defects, and Majorana fermions in chiral superconductors, Phys. Rev. B **86**, 100504(R) (2012).
[8] A. Mesaros, Y. B. Kim, and Y. Ran, Changing topology by topological defects in three-dimensional topologically ordered phases, Phys. Rev. B **88**, 035141 (2013).
[9] J. C. Y. Teo and T. L. Hughes, Existence of Majorana-fermion bound states on disclinations and the classification of topological crystalline superconductors in two dimensions, Phys. Rev. Lett. **111**, 047006 (2013).
[10] Z. Bi, A. Rasmussen, and C. Xu, Line defects in three-dimensional symmetry-protected topological phases, Phys. Rev. B **89**, 184424 (2014).
[11] W. A. Benalcazar, J. C. Y. Teo, and T. L. Hughes, Classification of two-dimensional topological crystalline superconductors and Majorana bound states at disclinations, Phys. Rev. B **89**, 224503 (2014).
[12] V. Parente, G. Campagnano, D. Giuliano, A. Tagliacozzo, and F. Guinea, Topological defects in topological insulators and bound states at topological superconductor vortices, Materials **7**, 1652 (2014).
[13] R.-J. Slager, A. Mesaros, V. Juričić, and J. Zaanen, Interplay between electronic topology and crystal symmetry: Dislocation-line modes in topological band insulators, Phys. Rev. B **90**, 241403 (2014).
[14] M. N. Chernodub and M. A. Zubkov, Chiral anomaly in Dirac semimetals due to dislocations, Phys. Rev. B **95**, 115410 (2017).
[15] A. Panigrahi, R. Moessner, and B. Roy, Non-Hermitian dislocation modes: Stability and melting across exceptional points, Phys. Rev. B **106**, L041302 (2022).
[16] F. Schindler, S. S. Tsirkin, T. Neupert, B. A. Bernevig, and B. J. Wieder, Topological zero-dimensional defect and flux states in three-dimensional insulators, Nat. Commun. **13**, 5791 (2022).
[17] S. S. Yamada, T. Li, M. Lin, C. W. Peterson, T. L. Hughes, and G. Bahl, Bound states at partial dislocation defects in multipole higher-order topological insulators, Nat. Commun. **13**, 2035 (2022).
[18] J. Paulose, B. G.-g. Chen, and V. Vitelli, Topological modes bound to dislocations in mechanical metamaterials, Nat. Phys. **11**, 153 (2015).
[19] H. Xue, D. Jia, Y. Ge, Y.-j. Guan, Q. Wang, S.-q. Yuan, H.-x. Sun, Y. D. Chong, and B. Zhang, Observation of dislocation-induced topological modes in a three-dimensional acoustic topological insulator, Phys. Rev. Lett. **127**, 214301 (2021).
[20] L. Ye, C. Qiu, M. Xiao, T. Li, J. Du, M. Ke, and Z. Liu, Topological dislocation modes in three-dimensional acoustic topological insulators, Nat. Commun. **13**, 508 (2022).
[21] Y. Deng, W. A. Benalcazar, Z.-G. Chen, M. Oudich, G. Ma, and Y. Jing, Observation of degenerate zero-energy topological states at disclinations in an acoustic lattice, Phys. Rev. Lett. **128**, 174301 (2022).
[22] F.-F. Li, H.-X. Wang, Z. Xiong, Q. Lou, P. Chen, R.-X. Wu, Y. Poo, J.-H. Jiang, and S. John, Topological light-trapping on a dislocation, Nat. Commun. **9**, 2462 (2018).
[23] J. Lu, K. G. Wirth, W. Gao, A. Heßler, B. Sain, T. Taubner, and T. Zentgraf, Observing 0D subwavelength-localized modes at ∼100 THz protected by weak topology, Sci. Adv. **7**, eabl3903 (2021).
[24] B.-Ye Xie, O. You, and S. Zhang, Photonic topological pump between chiral disclination states, Phys. Rev. A **106**, L021502 (2022).
[25] A. Agarwala and V. B. Shenoy, Topological insulators in amorphous systems, Phys. Rev. Lett. **118**, 236402 (2017).
[26] M. Geier, I. C. Fulga, and A. Lau, Bulk-boundary-defect correspondence at disclinations in rotation-symmetric topological insulators and superconductors, SciPost Phys. **10**, 092 (2021).
[27] Y. Liu, S. Leung, F.-F. Li, Z.-K. Lin, X. Tao, Y. Poo, and J.-H. Jiang, Bulk–disclination correspondence in topological crystalline insulators, Nature (London) **589**, 381 (2021).

[28] Y. Kubota, The bulk–dislocation correspondence for weak topological insulators on screw–dislocated lattices, J. Phys. A: Math. Theor. **54**, 364001 (2021).

[29] W. Brinkman, Magnetic symmetry and spin waves, J. Appl. Phys. **38**, 939 (1967).

[30] R. R. Birss, *Symmetry and Magnetism*, Series of Monographs on Selected Topics in Solid State Physics Vol. 3 (North-Holland, Amsterdam, 1964).

[31] V. L. Pokrovskii, Spin waves on dislocations, Pis'ma Zh. Eksp. Teor. Fiz. **11**, 233 (1970).

[32] A. N. Kuchko and M. V. Chernyshëva, Scattering of spin waves by a rectilinear edge dislocation, Phys. Solid State **40**, 1861 (1998).

[33] L. A. Turski and M. Mińkowski, Spin wave interaction with topological defects, J. Phys.: Condens. Matter **21**, 376001 (2009).

[34] S. G. Gestrin and E. A. Saĺnikova, Interaction of spin waves with dislocations in ferrodielectrics, Russ. Phys. J. **54**, 1177 (2012).

[35] V. G. Bar'yakhtar, M. A. Savchenko, and V. V. Tarasenko, Effect of dislocations on the line width of uniform ferro- and antiferromagnetic resonances, J. Exp. Theor. Phys. **27**, 858 (1968).

[36] J. Zmijan and J. Spalak, Ferromagnetic resonance line-width and shift by a group of dislocations, Solid State Commun. **35**, 699 (1980).

[37] M. Schmidt, Effect of dislocations on the ferromagnetic resonance linewidth, J. Phys. Colloq. **49**, C8-2069 (1988).

[38] J. Morkowski, Two magnon relaxation on dislocations in ferromagnets, Phys. Lett. A **26**, 144 (1968).

[39] J. Morkowski, Damping of the spin wave resonance by dislocations, J. Phys. Lett. **35**, 257 (1974).

[40] V. G. Bar'yakhtar, M. A. Savchenko, and V. V. Tarasenko, Relaxation and thermal conductivity in magnetic materials with dislocations, J. Exp. Theor. Phys. **24**, 623 (1967).

[41] A. Fomethe and G. A. Maugin, Influence of dislocations on magnon-phonon couplings, Int. J. Eng. Sci. **20**, 1125 (1982).

[42] M. Azhar, V. P. Kravchuk, and M. Garst, Screw dislocations in chiral magnets, Phys. Rev. Lett. **128**, 157204 (2022).

[43] Z.-X. Li, Y. Cao, and P. Yan, Topological insulators and semimetals in classical magnetic systems, Phys. Rep. **915**, 1 (2021).

[44] F. Zhuo, J. Kang, A. Manchon, and Z. Cheng, Topological phases in magnonics, Adv. Phys. Res. **4**, 2300054 (2023).

[45] Y. Onose, T. Ideue, H. Katsura, Y. Shiomi, N. Nagaosa, and Y. Tokura, Observation of the magnon Hall effect, Science **329**, 297 (2010).

[46] L. Zhang, J. Ren, J.-S. Wang, and B. Li, Topological magnon insulator in insulating ferromagnet, Phys. Rev. B **87**, 144101 (2013).

[47] A. Mook, J. Henk, and I. Mertig, Edge states in topological magnon insulators, Phys. Rev. B **90**, 024412 (2014).

[48] S. K. Kim, H. Ochoa, R. Zarzuela, and Y. Tserkovnyak, Realization of the Haldane-Kane-Mele model in a system of localized spins, Phys. Rev. Lett. **117**, 227201 (2016).

[49] R. Shindou, R. Matsumoto, S. Murakami, and J.-i. Ohe, Topological chiral magnonic edge mode in a magnonic crystal, Phys. Rev. B **87**, 174427 (2013).

[50] X. S. Wang and X. R. Wang, Topological magnonics, J. Appl. Phys. **129**, 151101 (2021).

[51] B. A. Bernevig and T. L. Hughes, *Topological Insulators and Topological Superconductors* (Princeton University Press, Princeton, NJ, 2013).

[52] M. Z. Hasan and C. L. Kane, *Colloquium:* Topological insulators, Rev. Mod. Phys. **82**, 3045 (2010).

[53] X.-L. Qi and S.-C. Zhang, Topological insulators and superconductors, Rev. Mod. Phys. **83**, 1057 (2011).

[54] X. S. Wang, A. Brataas, and R. E. Troncoso, Bosonic Bott index and disorder-induced topological transitions of magnons, Phys. Rev. Lett. **125**, 217202 (2020).

[55] Y. Akagi, Topological invariant for bosonic Bogoliubov–de Gennes systems with disorder, J. Phys. Soc. Jpn. **89**, 123601 (2020).

[56] H. D. Rosales and R. E. Troncoso, Robustness of topological magnons in disordered arrays of skyrmions, Phys. Rev. B **110**, 134435 (2024).

[57] G. Jackeli and G. Khaliullin, Mott insulators in the strong spin-orbit coupling limit: From Heisenberg to a quantum compass and Kitaev models, Phys. Rev. Lett. **102**, 017205 (2009).

[58] X. S. Wang, Y. Su, and X. R. Wang, Topologically protected unidirectional edge spin waves and beam splitter, Phys. Rev. B **95**, 014435 (2017).

[59] H. Kleinert, *Gauge Fields in Condensed Matter* (World Scientific, Singapore, 1989).

[60] J. Kim, K.-W. Kim, B. Kim, C.-J. Kang, D. Shin, S.-H. Lee, B.-C. Min, and N. Park, Exploitable magnetic anisotropy of the two-dimensional magnet CrI_3, Nano Lett. **20**, 929 (2020).

[61] P. Jiang, L. Li, Z. Liao, Y. X. Zhao, and Z. Zhong, Spin direction-controlled electronic band structure in two-dimensional ferromagnetic CrI_3, Nano Lett. **18**, 3844 (2018).

[62] T. Holstein and H. Primakoff, Field dependence of the intrinsic domain magnetization of a ferromagnet, Phys. Rev. **58**, 1098 (1940).

[63] J. H. P. Colpa, Diagonalization of the quadratic boson Hamiltonian, Physica A **93**, 327 (1978).

[64] T. A. Loring and M. B. Hastings, Disordered topological insulators via C*-algebras, Europhys. Lett. **92**, 67004 (2010).

[65] D. Toniolo, Time-dependent topological systems: A study of the Bott index, Phys. Rev. B **98**, 235425 (2018).

[66] D. Toniolo, On the Bott index of unitary matrices on a finite torus, Lett. Math. Phys. **112**, 126 (2022).

[67] For fermionic systems the metric $\eta = \mathbb{I}$ and the definition in the main text returns to the electronic Bott index.

[68] Z. Li, Y. Cao, P. Yan, and X. Wang, Higher-order topological solitonic insulators, npj Comput. Mater. **5**, 107 (2019).

[69] H. Zheng, Y. S. Meng, and Y. Zhu, Frontiers of *in situ* electron microscopy, MRS Bull. **40**, 12 (2015).

[70] Q. Yu, M. Legros, and A. M. Minor, *In situ* TEM nanomechanics, MRS Bull. **40**, 62 (2015).

[71] P. G. Callahan, B. B. Haidet, D. Jung, G. G. E. Seward, and K. Mukherjee, Direct observation of recombination-enhanced dislocation glide in heteroepitaxial GaAs on silicon, Phys. Rev. Mater. **2**, 081601(R) (2018).

[72] O. Schaff, A. K. Schmid, N. C. Bartelt, J. de la Figuera, and R. Q. Hwang, *In-situ* STM studies of strain-stabilized thin-film dislocation networks under applied stress, Mater. Sci. Eng. A **319-321**, 914 (2001).

[73] T. Tsuji and K. Yamanaka, Observation by ultrasonic atomic force microscopy of reversible displacement of subsurface

dislocations in highly oriented pyrolytic graphite, Nanotechnology **12**, 301 (2001).

[74] M. Telkhozhayeva and O. Girshevitz, Roadmap toward controlled ion beam-induced defects in 2D materials, Adv. Funct. Mater. **34**, 2404615 (2024).

[75] S. Pan, Y. Bai, J. Tang, P. Wang, Y. You, G. Xu, and F. Xu, Growth of high-quality CrI_3 single crystals and engineering of its magnetic properties via V and Mn doping, J. Alloys Compd. **908**, 164573 (2022).

[76] P. Meisenheimer, H. Zhang, D. Raftrey, X. Chen, Y.-T. Shao, Y.-T. Chan, R. Yalisove, R. Chen, J. Yao, M. C. Scott, W. Wu, D. A. Muller, P. Fischer, R. J. Birgeneau, and R. Ramesh, Ordering of room-temperature magnetic skyrmions in a polar van der Waals magnet, Nat. Commun. **14**, 3744 (2023).

[77] Y. Qi, M. A. Sadi, D. Hu, M. Zheng, Z. Wu, Y. Jiang, and Y. P. Chen, Recent progress in strain engineering on van der Waals 2D materials: Tunable electrical, electrochemical, magnetic, and optical properties, Adv. Mater. **35**, 2205714 (2023).

[78] X. Yu, Z. Peng, L. Xu, W. Shi, Z. Li, X. Meng, X. He, Z. Wang, S. Duan, L. Tong, X. Huang, X. Miao, W. Hu, and L. Ye, Manipulating 2D materials through strain engineering, Small **20**, 2402561 (2024).

[79] P. Andrich, C. F. de las Casas, X. Liu, H. L. Bretscher, J. R. Berman, F. J. Heremans, P. F. Nealey, and D. D. Awschalom, Long-range spin wave mediated control of defect qubits in nanodiamonds, npj Quantum Inf. **3**, 28 (2017).

[80] C. M. Purser, V. P. Bhallamudi, F. Guo, M. R. Page, Q. Guo, G. D. Fuchs, and P. C. Hammel, Spinwave detection by nitrogen-vacancy centers in diamond as a function of probe–sample separation, Appl. Phys. Lett. **116**, 202401 (2020).